American Mineralogist, Volume 89, pages 1078–1086, 2004

A novel approach to determine high-pressure high-temperature fluid and melt compositions using diamond-trap experiments

RONIT KESSEL,[1,*] PETER ULMER,[1] THOMAS PETTKE,[2] MAX W. SCHMIDT,[1] AND ALAN B. THOMPSON[1]

[1]Institut für Mineralogie und Petrographie, ETH-Zentrum, Zürich, Switzerland
[2]Institut für Isotopengeologie und Mineralische Rohstoffe, ETH-Zentrum, Zürich, Switzerland

ABSTRACT

We have developed a novel analytical technique for diamond-trap experiments to directly analyze high-pressure, high-temperature fluid and melt compositions in equilibrium with mantle material. Experiments were conducted at a pressure of 6 GPa and temperatures between 900–1200 °C in a multi-anvil apparatus with a synthetic K-free eclogite doped with 860 ppm Cs, ~20 wt% H_2O, and a layer of diamond aggregates serving as a fluid/melt trap. Experiments at identical conditions were analyzed with two different methods. In the new, "freezing," approach, the capsule was frozen prior to opening and kept frozen during laser-ablation ICP-MS analysis, thus ablating the quenched fluid (precipitates together with water that unmixed upon quenching) in a solid state. Cesium, fractionating completely into the fluid or melt phase, was used as an internal standard for calculating the fluid compositions. Calculated uncertainties on H_2O content in the fluid composition are 0.7–2.5%. In the conventional "evaporation" approach, water from the unmixed fluid was first evaporated from the capsule, then the remaining fluid precipitates were analyzed by LA-ICP-MS. The compositions of the residual eclogitic minerals were measured by electron microprobe, and the fluid composition was then determined by mass-balance. Uncertainties in mineral compositions lead to poor precision in fluid composition in this latter approach. Results of the two methods of fluid analysis were found to be in good agreement. Because the "freezing" approach analyzes the entire fluid directly and does not rely on mass balance for calculating fluid compositions, our new method provides a superior means for determining the composition of fluids. Secondly, it avoids loss of cations that remain soluble in water (e.g., Cs, K) after quenching the experiment.

INTRODUCTION

There is abundant evidence that C-H-O fluids are present in all magmas and rocks on Earth. Such evidence includes analyses of undegassed primitive lavas (e.g., Harris and Anderson 1984; Stolper and Newman 1994), fluid inclusions in upper mantle minerals (Izraeli et al. 2001; Scambelluri and Philippot 2001), and the composition of volatile-bearing minerals in mantle xenoliths (e.g., Brenan and Watson 1991). These studies indicate that H_2O is the dominant volatile component in the upper mantle. The presence of aqueous fluids plays an important role in many processes in the Earth's mantle. For example, it affects the melting and crystallization behavior of silicates (e.g., Yoder and Kushiro 1969; Wyllie and Ryabchikov 2000) and thus has significant consequences for the depth, temperature, and composition of melting. In addition, under mantle conditions, fluid dissolves significant amounts of matter and is mobile, thus acting as an agent of mass transfer between mantle reservoirs and crust (e.g., McCulloch and Gamble 1991; Hawkesworth et al. 1993). Therefore, fluids play a major role in mantle differentiation through metasomatism and melting, but the exact composition of fluids in the mantle and their metasomatic effects remain largely unknown.

Experiments are a powerful tool to investigate fluid transport in the mantle and its effect on melting and metasomatism. Many experimental studies have investigated the composition of high-pressure, high-temperature (HP-HT) fluids and hydrous melts in equilibrium with mantle material (e.g., Manning 1994; Rapp and Watson 1995; Haifei 1996; Green et al. 2000). However, melt- and fluid-bearing experiments at HP-HT are not easy to perform. Manning (1994) used a double-capsule technique collecting the fluid in the outer capsule. However, these experiments require large capsules and are, therefore, limited to lower pressures. At higher pressure, traditionally, a capsule containing solid material and water is exposed to HP-HT and, after quenching, is mounted in epoxy to examine the run products (Stern and Wyllie 1978; Rapp and Watson 1995; Yaxley and Green 1998). The difficulty with this approach is that the melt or fluid at the experimental condition undergoes extensive crystallization and/or exsolution upon quenching. In experiments on dry or fluid-undersaturated systems, the melt converts upon quenching to glass, with or without recrystallization, depending on the composition and the experimental conditions. In fluid-rich systems, a considerable amount of silicates is dissolved in the fluid phase at HP-HT. Upon quenching, the fluid tends to exsolve into water and precipitates. Thus, the recognition of the original melt or fluid and the determination of its composition are often impossible in this traditional experimental approach. A reliable data set on fluid and hydrous-melt compositions coexisting with mantle material at

* E-mail: kessel@erdw.ethz.ch

HP-HT is, therefore, lacking.

Kushiro and Hirose (1992) and Baker and Stolper (1994) independently developed an experimental technique to circumvent the quenching problem to allow the direct determination of the melt composition coexisting with solid material at HP-HT. The idea behind this technique is similar to that used by Ryabchikov and Boettcher (1980). A thin layer of diamond powder is placed inside the sample capsule in contact with the solid starting material, such that the mobile melt produced during the experiment fills the voids in between the diamonds. On quenching, even if the melt trapped in between the diamonds undergoes crystallization, the bulk composition of the melt in the diamond trap is unchanged. The melt composition can then directly be determined by analyzing the diamond-trap.

The application of the diamond-trap technique was later extended to study wet systems where aqueous fluid is in equilibrium with the solid material composition (Stalder et al. 2000, 2001, 2002). Stalder et al. (2000, 2001) applied the diamond-trap technique to study the fluid composition in the systems albite-H_2O and MgO-SiO_2-H_2O at upper mantle conditions, respectively. After the experiment, the capsule was pierced to let the water out and then mounted in epoxy and polished to expose a longitudinal section through the experimental charge exposing both the residual solid and the diamond trap. This approach is referred to here as the "evaporation" approach. Stalder et al. (2000, 2001) analyzed the diamond trap by using Laser Ablation-Inductively Coupled Plasma-Mass Spectrometry (LA-ICP-MS) with Ni and C from the diamonds forming the trap as internal standards, and calculated the fluid composition using a reference experiment in which the amount of dissolved silicates in the fluid was known independently.

A prerequisite in the "evaporation" method of calculating fluid composition is that the unmixed water, which is evaporated from the capsule before analysis, is pure H_2O and all the dissolved material in the fluid at run condition resides as precipitates. In many subsystems this assumption is valid. For example, Stalder et al. (2001) demonstrated that no fractionation occurred while opening the capsule by comparing the loss of weight due to evaporation of the water to the weight of H_2O originally put in the capsule. However, in chemical systems representing natural compositions, this assumption is not always valid. In a later study, Stalder et al. (2002) studied the K_2O-MgO-Al_2O_3-SiO_2-H_2O system. After piercing the capsule, the escaping solution appeared cloudy, had a highly basic pH of 14, and left a white precipitate around the pierced hole after water was evaporated. In addition, the weight loss due to drying was greater than the original amount of H_2O added to the capsule. These observations indicated that not all the ions dissolved at run conditions precipitated upon quenching, but a fraction of them remained dissolved in the water and escaped from the capsule. Additionally, mass-balance calculations suggested that the escaping solution is highly alkaline, containing mainly K. The loss of material during preparation of the capsule prevented Stalder et al. (2002) from calculating fluid compositions.

We developed a novel analytical technique to allow determination of fluid and hydrous melt compositions trapped in between diamond aggregates in any system regardless of its composition. In the new approach, referred to here as the "freezing" approach, the capsule is frozen before being opened and maintained frozen *during* the analyses, so that the HP-HT fluid is analyzed as a solid. To demonstrate the validity of the new approach, we chose a chemical system where both the "evaporation" and the "freezing" approaches can be applied, i.e., the K-free basalt + water system. We determined the fluid composition using both approaches and compared the results.

Experimental procedure and analytical techniques

Starting materials

The starting material consisted of a synthetic basaltic powder. We chose a K-free basaltic composition (TB-1) of Schmidt and Poli (1998) as a representative mid-ocean ridge basalt (MORB) composition (see Table 1). Schmidt and Poli (1998) studied the H_2O-saturated phase diagram of this composition at pressures up to 120 kbars and temperatures of 875 °C (representing subduction zone conditions), to investigate the formation of volcanic arcs. Reagent grade SiO_2, TiO_2, Al_2O_3, Fe_2O_3, and MgO, were sintered in Al_2O_3 crucibles at 800 °C for 15 h; $CaCO_3$ was dried at 400 °C and Na_2SiO_3 at 300 °C in Al_2O_3 crucibles for 20 hours. The dried oxides were mixed to yield the TB-1 composition and ground in a silica mortar for 2 hours. A Pt crucible was pre-equilibrated with Fe suited to MORB following the procedure given by Kessel et al. (2001). The pre-saturated Pt crucible containing the oxide mix was suspended from a sample holder at the hot spot of a vertical furnace, and held in a flowing H_2-CO_2 gas at 1300 °C [~80 °C above the liquidus calculated using the MELTS program (Ghiorso and Sack 1995)] and $\log_{10} f_{O_2} = -6.87$ (QFM + 0.49) for 6 h to produce a basaltic glass with an Fe^{3+}/Fe^{2+} ratio of ≈0.10 [calculated with the algorithm of Kress and Carmichael (1988)]. The basaltic glass was extracted from the Pt crucible and ground to a powder. Homogeneity and the degree to which oxides were converted to basalt were determined using electron microprobe analyses. No Fe loss to the Pt crucible was detected. The composition of the basaltic glass produced in this study and that of TB-1 by Schmidt and Poli (1998) are given in Table 1.

The basaltic starting material was doped with 860 ppm Cs to have an internal standard for quantification of LA-ICP-MS analyses of the diamond trap. Cesium is a highly incompatible element in K-free eclogite (mica-free), and therefore resides preferably in the fluid or melt phase. Cesium was added to the powder as CsOH dissolved in 50% H_2O. The Cs-doped basaltic powder was then dried at 110 °C for one hour. To verify the amount of Cs in the powder and its homogeneous distribution, ten aliquots of 9.5–40 mg Cs-doped basaltic powder were dissolved in HF-HNO_3 and were analyzed for Cs on an ELAN 6100 ICP-MS. Between 85 and 100% of the calculated Cs in the basalt was measured in all aliquots, confirming the initial amount of Cs in the starting material. The uncertainty on the amount of Cs in each capsule is taken as 5% (1σ).

The experiments were performed using Au capsules (2.3 mm outer diameter, 2.0 mm inner diameter). First, 2.1–3.4 μL H_2O were added to the capsule (measured with a micropipette and confirmed by weight), corresponding to 17–26 wt% of the basalt + water system. The capsule was then filled with ~3–5 mg Cs-doped basalt powder, followed by a thin layer of synthetic diamond aggregates (1.2–3.1 mg of 15–25 μm diameter grains), and another layer of ~3–5 mg Cs-doped basalt powder (total weight of basalt powder: 7.2–12.2 mg). The diamonds constituted 9–24 wt% of the material loaded into the capsule. The capsule was welded while frozen (using liquid nitrogen), and the weight of the capsule was compared before and after welding to ensure no loss of water during welding. The sealed capsule was squeezed to a final cylindrical shape with a length of 2–3 mm.

Table 1. Composition of starting material

oxide	TB-1* (wt%)	Initial mix† (wt%)
SiO_2	51.58	50.41(1.27)
TiO_2	1.52	1.47(7)
Al_2O_3	16.68	16.89(25)
FeO	9.96	10.09(95)
MgO	7.02	6.85(36)
CaO	9.90	9.96(37)
Na_2O	3.16	3.26(19)
total	99.82	98.92

Note: Numbers enclosed in parentheses indicate one standard deviation of the distribution of analyses.
* Composition taken from Schmidt and Poli (1998). All Fe expressed as FeO.
† Average of 18 analyses of basaltic glass (electron probe analyses).

Experimental conditions

Experiments were conducted in a 600-ton Walker-type multi-anvil apparatus (Walker 1991; Walker et al. 1993). High-temperature pressure calibration experiments were performed on the following phase transitions: quartz-coesite (3.2 GPa at 1200 °C; Bose and Ganguly 1995); fayalite-γFe_2SiO_4 (5.0 GPa at 1000 °C; Yagi et al. 1987); $CaGeO_3$ garnet-perovskite (6.1 GPa at 1000 °C; Susaki et al. 1985); and coesite-stishovite (9.1 GPa at 1000 °C; Yagi and Akimoto 1976). Pressure is estimated to be accurate to within ±0.2 GPa. Temperature was measured using a Pt_6Rh-$Pt_{30}Rh$ (type B) thermocouple; reported temperatures are not corrected for the effect of pressure on the thermocouple EMF. During the runs, temperature was kept constant to within ±3 °C and the applied load to ± 1 ton.

Experiments were conducted at 6 GPa and temperatures between 900 and 1200 °C for 2–7.5 h. Experiments were performed using 19 mm edge length MgO octahedra [fabricated from MgO-based castable ceramics (Ceramcast 584)] and tungsten carbide cubes with truncation edge length (TEL) of 12 mm. The Au capsule was placed in a boron-nitride cylinder inside a 4.0 mm outer diameter stepped graphite furnace. MgO spacers and Mo caps were placed above and below the capsule to ensure contact between the furnace and the cubes. Care was taken to place the capsule in the center of the assembly (the hot spot of the graphite furnace). The thermocouple was inserted radially through the octahedron gaskets and furnace, and placed at the bottom of the capsule. Temperatures reported in this study are thermocouple readings. The experimental conditions are listed in Table 2.

Oxygen fugacity was not controlled in these experiments but limited between the f_{O_2} imposed by the initial Fe^{3+}/Fe^{2+} ratio in the starting material (≈ 0.10) and that imposed by the diamond-fluid equilibrium (C-COH buffer, H_2O-maximum), as potential oxidation of the charge by hydrogen loss was prevented by the use of boron-nitride surrounding the capsule (Truckenbrodt et al. 1997). However, we reckon that the f_{O_2} remains close to the f_{O_2} imposed by the initial Fe^{3+}/Fe^{2+} ratio because diamonds are highly unreactive, as discussed by Stalder et al. (2001).

Stalder and Ulmer (2001b) ran experiments containing hydrous phases at pressures of 5-14 GPa and temperatures of 800–1200 °C, and observed a strong compositional zonation in the charges. Such chemical differentiation within the capsule can lead to misinterpretation of the mineral stabilities and reaction directions in the experiments. Schmidt and Ulmer (2004) explained the chemical differentiation in such "static" experiments as a result of the temperature gradients in the capsule (causing Soret diffusion in the fluid). To circumvent this effect, Schmidt and Ulmer (2004) mounted a multi-anvil on a rocking device enabling the apparatus to be turned vertically 180 ° while maintaining pressure and temperature. Turning the apparatus for the duration of the experiment results in frequent inversion of the charge in the gravitational field leading to re-homogenization and migration of the fluid phase along the vertical axis of the capsule. This rocking multi-anvil in turn results in a more-equilibrated phase assemblage and enhancement of reaction rates. In our diamond-trap experiments, we rock the multi-anvil apparatus 180 ° every 15 minutes during the experiment to improve the extent of equilibrium between the water and the residual solid and to reduce the chemical zonation along the capsule due to thermal and density effects.

The experiments were terminated by first turning off the furnace power, followed by unloading pressure over 10 hours. Once unloaded, the octahedron was retrieved and the position and length of the capsule were measured carefully to determine the temperature profile experienced by the capsule during the experiment (Table 2). The temperature gradient over the capsule length is calculated to be 21 °C on average (ranging from 18–23 °C) employing a thermal gradient of 11 °/mm along the stepped graphite furnace, as estimated for a similar assemblage by Konzett et al. (1997).

TABLE 2. Run conditions and analytical methods for experiments run at 6 GPa and temperatures between 900 and 1200 °C

Run	*T* (°C)*	*T* gradient†	Duration (h)	Silicate (mg)	Water added (mg)	Water added (wt%)‡	Analytical method
RK31	900	18	7.5	9.5	3.4	26	"freezing"
RK45	900	20	6	9.5	2.1	18	"freezing"
RK39	900	20	7	8.6	2.4	22	"evaporation"
RK42	1000	21	4	8.6	2.4	22	"freezing"
RK33	1000	20	7	8.1	2.6	24	"evaporation"
RK47	1000	23	5	12.2	2.5	17	"evaporation"
RK27	1100	23	2	7.5	2.4	24	"freezing"
RK26	1100	23	4	8.4	2.4	22	"evaporation"
RK32	1200	22	5	8.6	2.3	21	"freezing"
RK44	1200	21	3	10.1	2.5	20	"freezing"
RK29	1200	20	5	7.9	2.4	23	"evaporation"
RK40	1200	21	4	7.2	2.5	26	"evaporation"

* Temperature gradient along the capsule is calculated assuming a thermal gradient of 11 °/mm (see text).
† Temperatures are those registered by the thermocouple placed at the bottom of the capsule.
‡ wt% of water in the basalt+water system.

Analytical techniques

Experimental charges were examined using a LEO 1530 scanning electron microscope (SEM). An example of a back-scattered electron (BSE) image of a capsule run at 6 GPa and 1100 °C shows the diamond layer sandwiched between eclogitic material (Fig. 1a). The residual eclogite in all experiments consisted of garnet, clinopyroxene, coesite, kyanite, and rutile. Figure 1b is a close up BSE image of the diamond trap shown in Figure 1a filled with precipitates. Veins of precipitates extend from the diamond layer into the eclogite. This observation indicates that the fluid volume was larger than the trap volume, allowing constant flow of fluid through the eclogite. It also demonstrates that it would be inadequate to analyze or physically separate "bulk eclogite" to determine bulk eclogite/fluid partition coefficients, as the bulk eclogite would invariably be contaminated by fluid phase.

The fluid or hydrous melt phase at run conditions exsolves upon quenching to liquid water and precipitates. Hydrous phases were not found in the eclogite suggesting that all of the H_2O originally added to the starting material reside in the

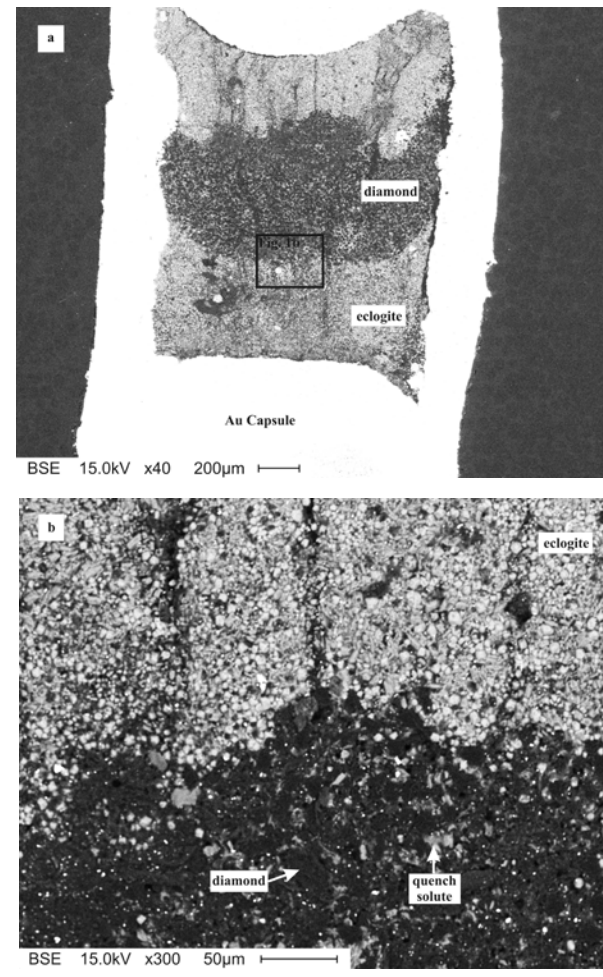

FIGURE 1. (**a**) Back-scattered electron (BSE) image of an experimental charge containing eclogite + diamonds + water (RK26, 6 GPa, 1100 °C) showing the diamond layer sandwiched between eclogitic layers. (**b**) BSE image of the boundary between the diamond trap and the eclogitic residue in the same experiment, showing the diamond aggregates and the precipitates trapped in between them.

fluid/melt before quenching. To determine the composition of the fluid or melt, two sets of experiments were conducted at identical *P-T* conditions. One set of experiments was analyzed following the "evaporation" approach and the other following the "freezing" approach. The results of the two sets were compared.

Capsules treated following the "evaporation" approach were prepared for analyses following the procedure from Stalder et al. (2001). After termination of the experiment, the capsule was weighed, pierced, dried at 110 °C for ~15 minutes, and weighed again. The difference in weight was compared to the amount of H_2O originally added to the capsule. In all experiments analyzed following the "evaporation" approach, a mass corresponding to 90–100% of the originally added H_2O was evaporated, verifying the existence of a closed system during the course of the experiment and almost complete unmixing of the H_2O upon quenching. The uncertainty on the amount of H_2O in the capsule is therefore taken as 5% (1σ). The capsule was then mounted longitudinally in epoxy and polished to expose a maximum surface of the charge including the eclogite and diamond layer. Due to the fluid-saturated conditions of the experiments, and the release of the fluid at the end of the experiment, grain coherence was poor. The exposed surface was multiply impregnated with epoxy and carefully polished to expose a section of the capsule as complete as possible (Fig. 1a). The mounted capsule was placed in a sample holder inside a standard laser-ablation (LA) stage chamber together with a small piece of an external standard NIST-SRM-610, and put on a table of petrographic microscope connected to a TV screen.

For the "freezing" approach, a modified LA sample holder and stage were built (Fig. 2). A brass sample holder was placed on a metal plate mounted to the LA stage. A U-shaped channel is located in the metal plate beneath sample. One exit of the channel was connected via a tube to a liquid nitrogen source and the other to a pump. When a capsule was placed on the stage, liquid nitrogen was pumped through the channel freezing the capsule together with the sample holder. The stage was initially placed inside a dry air box constantly flushed with Ar or N_2 to reduce the humidity in the box and to prevent condensation of icelets from ambient air on the capsule within the ablation chamber. Once the capsule was frozen it was cut open using a razor blade to expose a longitudinal section of the capsule. A small piece of NIST-SRM-610 was also positioned on the sample holder, and the glass cover of the LA chamber was put in place while flushing the chamber with He carrier gas. The LA chamber, containing the opened capsule and the external standard, was then placed on the stage of the LA microscope for analysis. Care was taken to keep the capsule constantly frozen during all steps, preventing any fraction of the fluid to be lost from the experimental product upon opening the capsule and during analyses. Argon gas was continuously flushed across the outside of the glass cover to prevent ice formation, to maintain clear visibility of the capsule through the microscope, and to ensure maximum laser beam transmission through the ablation chamber glass.

The diamond trap in both approaches was analyzed using the LA-ICP-MS. Reflected light was essential to locate the diamond trap and distinguish it from the surrounding eclogite and to adjust the pit size of the ablating laser according to the shape of the diamond layer. Three to seven analyses were done along the diamond layer. A detailed description of the instrument and the operation conditions are given in Halter et al. (2002). A pulsed 193 nm ArF excimer laser with an energy homogenized beam profile was used (Günther et al. 1997). The ablated aerosols were carried to the ICP-MS by He carrier gas. Analyses were done using an ELAN 6100 quadrupole mass spectrometer in dual detector mode. Data were acquired in blocks of up to 16 individual sample analyses bracketed by two analyses of the NIST-SRM-610. Analyses were carried out at ~100 mJ laser output energy and 10 Hz. Dwell time was between 10 to 20 ms, and the quadruple settling time between measurements was 3 ms. Background was taken for 40–50 seconds and the sample signal was collected for 10–30 seconds. The largest suitable ablation spot (60–110 μm diameter) was used to analyze the diamond trap to obtain the best averaging during sampling of the experimental product interstitial to the ~20 μm sized diamonds.

We analyzed for ^{29}Si, ^{49}Ti, ^{27}Al, ^{25}Mg, ^{57}Fe, ^{42}Ca, ^{23}Na, and ^{133}Cs. Data reduction followed procedures described in Longerich et al. (1996). The background and signal time intervals were set manually to calculate the gross count rates of each element in each analysis. The background count rates were subtracted from the signal count rates to give the background-corrected signal count rates for each element in each individual analysis. The average intensities measured on the two bracketing external standard analyses provided sensitivities corrected linearly for instrumental drift during the acquisition of one analytical block. Figure 3a shows a typical LA-ICP-MS intensity profile as a function of time for a few elements from the diamond trap in a capsule treated following the "evaporation" approach, and Figure 3b in a capsule treated following the "freezing" approach.

The choice of signal intervals for the "evaporation" run products was always at the beginning of the signal (Fig. 3a), because the diamond layer could be recognized easily in these polished samples (Fig. 1a). In contrast to this, "freezing" run products were cut open with a razor blade, thereby often smearing eclogite grains onto the diamond layer. Therefore, signal intervals were often taken after discarding the first 20–30 seconds of signal during which the contaminated surface was ablated (Fig.

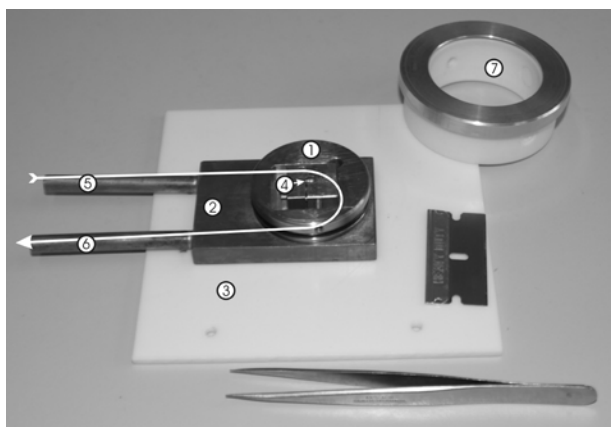

FIGURE 2. Picture of the modified laser-ablation (LA) stage that enables freezing of the capsule prior to opening it and maintaining it frozen during analyses. (1) brass sample holder; (2) metal (copper) plate; (3) LA stage; (4) capsule; (5) entrance to liquid nitrogen source; (6) exit to a pump; (7) ablation chamber. Curve indicates flow of liquid nitrogen through the channel inside the metal plate.

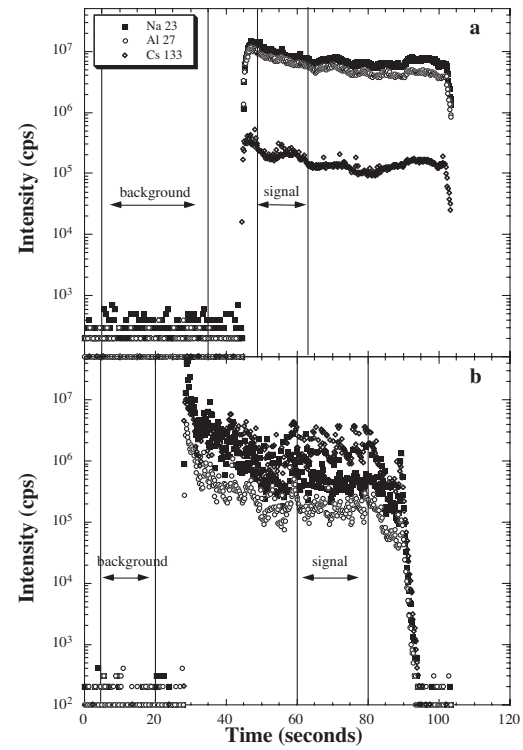

FIGURE 3. Typical LA-ICP-MS intensity vs. time profiles for Na, Al, and Cs. The areas marked "background" and "signal" were selected as integration intervals for the analysis. (**a**) Signal of the diamond trap in a capsule treated following the "evaporation" approach using 110 μm diameter laser beam (RK26, 6 GPa, 1100 °C). (**b**) Signal of the frozen fluid in a capsule treated following the "freezing" approach using 75 μm diameter laser beam (RK45, 6 GPa, 900 °C).

3b). An obvious difference between the signals of the two approaches is that signals from the "evaporation" approach are comparatively smooth whereas those of the "freezing" approach exhibit much more intensity scatter. This difference relates to the fact that the diamond layer in the "evaporation" approach was embedded with epoxy to allow for polishing the sample, thereby keeping the diamond aggregates well together and providing a matrix for the evaporates, whereas in the "freezing" approach, diamonds were only held together by frozen fluid. As a consequence, variability in ablation rate was much more pronounced in the "freezing" approach, resulting in the more variable signal. Average signal intensities are not affected by this, however, since each isotope was measured sufficiently often (i.e., more than ~100 times) per signal integration interval, hence representative sampling is ensured (Pettke et al. 2000).

Element ratios of the experimental product in both approaches were obtained from the LA-ICP-MS analysis by external standardization only, and assuming that none of the analytes of interest are contained in the synthetic diamonds. Internal standardization was then used to convert the apparent element concentrations into true values by determining the relative sensitivity factor via an internal standard [see Halter et al. (2002) for details]. The weight fraction of diamonds in each ablation spot thereby is not of importance, as all the analytes of interest are exclusively contained in the precipitates or fluid (i.e., the diamonds simply dilute the signal and the internal standard automatically accounts for this). Moreover, hydrogen cannot be analyzed by LA-ICP-MS. Therefore, the precipitate composition in each ablation spot can be combined with the amount of H_2O added into the capsule initially, resulting in element concentrations in the fluid. Details of these quantification procedures for the "evaporation" and the "freezing" approaches are outlined below.

The eclogite mineral compositions in a separate set of experiments (see below) were analyzed using a CAMECA SX50 electron microprobe with an accelerating voltage of 15 keV and a beam current of 20 nA. Counts were collected for 20 seconds on peak and 10 seconds at each background position except for Na, where the signal was collected for only 10 seconds on the peak and 5 on the background. Garnet and pyroxene were analyzed for Si, Ti, Al, Mg, Fe, Ca, and Na using wollastonite (for Si and Ca), hematite (for Fe), aegirine (for Na), rutile (for Ti), K-feldspar (for Al), and periclase (for Mg) as standards.

Calculation of fluid and solid compositions

Eclogite mineral compositions

The eclogitic mineral assemblages in all experiments contained garnet, clinopyroxene, coesite, kyanite, and rutile. The presence of a high-pressure mineralogy in all experiments confirmed the complete conversion of the original basaltic glass starting material to an equilibrated eclogitic assemblage under the experimental conditions. However, due to the presence of the diamond layer, the experimental charge could not be polished well enough to allow determination of the eclogitic mineral compositions adjacent to the diamond layer using the electron microprobe. The mineral compositions in the residual eclogite were therefore determined from a separate set of experiments. Capsules containing basaltic powder and water (without diamonds) were ran at 6 GPa and temperatures between 900 and 1200 °C for 6–9 hours. The f_{O_2} in this set of experiments was constrained by the initial Fe^{3+}/Fe^{2+} ratio of the starting material (≈ 0.10, close to QFM), provided that boron-nitride surrounding the capsule prevented hydrogen loss from the charge. Despite the absence of diamond in these experiments, the f_{O_2} in the two sets should be similar because reduction due to reaction with diamonds under similar conditions was shown to be negligible (Stalder et al. 2001). The multi-anvil apparatus containing these experiments also was turned 180° every 15 minutes, identical to the procedure taken with the diamond-trap experiments. At the end of each experiment, the capsule was retrieved, pierced, and dried to allow the water to evaporate. The capsule was then mounted in epoxy and polished to expose a longitudinal section of the capsule. Garnet, pyroxene, and coesite appear as large crystals distributed homogenously along the capsule. Rutile and kyanite appear as inclusions in garnet and pyroxene. The average and standard deviation of garnet and pyroxene compositions from each temperature are given in Table 3. The kyanite and rutile inclusions are too small to be analyzed accurately and we therefore used ideal compositions for both phases in our mass-balance calculations.

"Evaporation" approach

In the "evaporation" approach, the capsule is opened after the experiment, allowing the unmixed liquid water to evaporate. It is assumed that only H_2O evaporated from the capsule leaving all the ions originally dissolved in the fluid as precipitates trapped in between the diamond aggregates. This assumption is based on the close to 100% weight loss of H_2O at the end of the experiment and the clear appearance of the water released from the capsule upon piercing.

First, we assume that the sum of the oxides of Si, Ti, Al, Mg, Fe, Ca, and Na (except H_2O) analyzed in the diamond trap is 100% and calculate the anhydrous composition of the precipitates. In all our calculations, all Fe was taken as Fe^{2+}. Secondly, we perform a mass-balance calculation on the residual eclogite phases and the precipitates; the initial mass of each oxide in the starting material is distributed at the end of the experiment among the minerals in the residual eclogite and the precipitates according to the mass fractions of each phase. We perform an iterative least-squares calculation to determine the weight fraction and mass of each of the phases in the mass balance (i.e., garnet, cpx, coesite, rutile, kyanite, precipitates) best fitting all the oxides simultaneously. The amount of H_2O is then added and combined with the weight fraction of precipitates the fluid composition is calculated. Four to seven spots were analyzed along the diamond layer and the average and standard deviation of the calculated fluid compositions at each temperature are given in

Table 3. Mineral composition and proportions in eclogite at 6 GPa and temperatures between 900 and 1200 °C

T (°C)	900		1000		1100		1200	
Run	Grt (10) *	CPX (7)	Grt (10)	CPX (10)	Grt (7)	CPX (7)	Grt (15)	CPX (9)
SiO_2	40.99(1.08) †	59.99(75)	39.42(76)	56.47(62)	39.81(1.07)	57.47(42)	39.72(30)	56.76(31)
TiO_2	1.44(67)	0.15(20)	1.11(40)	0.22(12)	1.12(23)	0.20(1)	1.05(33)	0.37(16)
Al_2O_3	19.85(1.31)	16.51(1.03)	20.88(67)	14.44(71)	21.29(75)	16.05(33)	21.37(72)	13.78(58)
FeO	17.86(3.51)	2.06(46)	18.42(3.07)	4.81(2.50)	15.40(2.29)	2.08(25)	15.83(1.14)	3.09(1.00)
MgO	7.85(1.90)	5.00(92)	9.66(1.59)	6.36(43)	10.55(1.35)	5.91(41)	9.42(128)	6.97(32)
CaO	12.06(52)	7.62(33)	11.50(1.34)	10.57(45)	11.75(61)	8.52(51)	12.61(1.46)	10.36(46)
Na_2O	0.20(2)	8.66(36)	0.13(4)	7.55(40)	0.21(5)	9.38(29)	0.23(8)	8.29(34)
total	100.25	100.00	101.10	100.41	100.13	99.61	100.24	99.64

* Numbers enclosed in parentheses indicate total number of analyses.
† Numbers are wt% (electron probe analyses). Numbers enclosed in parentheses indicate absolute one standard deviation of the distribution of average grain compositions.

TABLE 4A. Fluid compositions in equilibrium with eclogite at 6 GPa and temperatures between 900 and 1200 °C determined following the "evaporation" approach

T (°C)	900	1000	1000	1100	1200	1200
Run	Rk39(5)*	RK33(5)	RK47(5)	RK26(4)	RK40(7)	RK29(6)
SiO_2†	9.33(4.72)‡	14.54(4.97)	25.18(3.92)	31.64(4.84)	26.00(1.16)	27.32(2.20)
TiO_2	0.06(3)	0.25(6)	0.58(4)	0.86(14)	1.02(3)	1.02(6)
Al_2O_3	0.83(40)	1.56(35)	3.50(54)	4.41(76)	6.51(19)	5.72(38)
FeO	0.15(8)	0.60(12)	0.86(20)	1.13(20)	2.24(9)	1.92(9)
MgO	0.25(12)	0.58(11)	1.03(23)	1.11(21)	1.91(7)	1.61(9)
CaO	0.76(73)	1.89(15)	3.70(25)	2.78(70)	4.42(15)	3.84(45)
Na_2O	1.00(56)	0.38(15)	2.37(27)	2.07(44)	3.30(19)	4.15(12)
H_2O	87.47(6.55)	79.97(5.69)	62.75(5.36)	55.99(5.88)	54.59(1.57)	54.28(2.89)
Cs/Si (wt)§	0.012(2)	0.007(1)	0.003(2)	0.0005(1)	0.0004(3)	0.0037(8)
Mineral fractions in eclogite						
garnet	0.59(2)	0.50(2)	0.55(2)	0.77(5)	0.77(2)	0.78(3)
cpx	0.37(1)	0.44(1)	0.38(1)	0.21(2)	0.13(2)	0.12(1)
coesite	0.03(1)	0.03(2)	0.04(1)	0.01(3)	0.10(1)	0.09(1)
rutile	0.007	0.010	0.009	0.006	0.004	0.004
kyanite	0.000	0.018	0.020	0.000	0.000	0.004
Total dissolved silicates (%)						
	12.53(6.55)	20.03(5.69)	37.25(5.36)	44.01(5.88)	45.41(1.57)	45.72(2.89)

* Numbers enclosed in parentheses indicate total number of analyses. Points were analyzed across the diamond layer.
† Fluid compositions are normalized to 100%.
‡ Numbers are wt%. Numbers enclosed in parentheses indicate absolute one standard deviation of the average of analyses.
§ Average elemental Cs/Si (by wt) calculated from the LA-ICP-MS signal.

TABLE 4B. Fluid compositions in equilibrium with eclogite at 6 GPa and temperatures between 900 and 1200 °C determined following the "freezing" approach

T (°C)	900	900	1000	1100	1200	1200
Run	RK31(3)*	RK45(5)	RK42(5)	RK27(7)	RK32(4)	RK44(7)
SiO_2†	9.22(9.80)‡	14.61(1.37)	22.87(5.26)	29.40(2.10)	20.69(4.02)	24.27(1.43)
TiO_2	0.08(1)	0.13(3)	0.19(3)	0.92(19)	1.21(5)	0.99(17)
Al_2O_3	0.63(11)	1.00(24)	1.38(36)	3.34(75)	4.93(208)	5.37(58)
FeO	0.25(11)	0.34(12)	0.53(24)	1.32(44)	2.45(1.00)	2.30(15)
MgO	0.22(2)	0.43(11)	0.45(10)	0.84(16)	1.71(81)	1.55(13)
CaO	0.54(11)	1.49(36)	1.60(27)	3.02(76)	4.11(1.60)	4.60(89)
Na_2O	1.36(38)	0.92(32)	1.26(16)	1.57(26)	1.95(42)	4.35(50)
H_2O	87.71(1.68)	81.08(2.35)	71.71(6.07)	59.59(3.97)	62.96(9.81)	56.57(1.32)
Cs/Si (wt)§	0.049(6)	0.070(8)	0.022(6)	0.012(2)	0.022(7)	0.017(1)
Total dissolved silicates (%)						
	12.29(1.68)	18.92(2.35)	28.29(6.07)	40.41(3.97)	37.04(9.81)	43.43(1.32)

Numbers enclosed in parentheses indicate total number of analyses. Points were analyzed across the diamond layer.
* Fluid compositions are normalized to 100%.
‡ Numbers are wt%. Numbers enclosed in parentheses indicate absolute one standard deviation of the average of analyses.
§ Average elemental Cs/Si (by wt) calculated from the LA-ICP-MS signal.

Table 4a. Also given are the weight fractions of each mineral in the eclogite and the amount of total dissolved silicates in the fluid. The standard deviation on the average amount of H_2O ranges from 3.2 to 8.0%, demonstrating a high degree of homogeneity of the fluid trapped in the diamond-trap in all experiments. The homogeneous fluid composition along the diamond trap together with the complete conversion of the basaltic starting material to an eclogitic assemblage demonstrate that the system approached equilibrium during the experimental duration.

To evaluate the uncertainty on the fluid composition due to the uncertainties in the compositions of phases used in the mass balance, we used a mass-balance program propagating errors on individual phases and bulk compositions through Monte Carlo error propagation. The average and standard deviations of the starting material (Table 1), residual eclogitic mineral compositions (Table 3), and the average composition of the precipitates in each experiment were used to run 10,000 Monte-Carlo cycles to determine the best fit and uncertainty on the mass fractions of each phase. The errors on the mass fractions derived by the program and the error on the amount of H_2O in each experiment (5%) were then propagated to calculate the uncertainty on the fluid composition. The uncertainty on the amount of H_2O in the fluid ranges between 30–100%. These large uncertainties are due to the large standard deviations on the average compositions of the residual minerals in the eclogite in each experiment.

"Freezing" approach

In the "freezing" approach, the capsule is frozen prior to being opened and is kept frozen during laser ablation analyses of the diamond trap (diamonds+frozen fluid). The purpose of freezing the capsule is to prevent the escape of any elements that remained dissolved in the unmixed water phase while opening the capsule.

The LA-ICP-MS technique provides accurate element ratios that require calibration by an independently known internal standard to convert to absolute concentrations. To determine the fluid composition in this approach, we used the Cs added to the starting material as an internal standard. Cesium is a highly incompatible element in K-free eclogite systems (i.e., mica-free), and therefore resides preferably in the fluid or melt phase. No studies have been done to estimate the partition coefficient of Cs between eclogite and fluid at our experimental conditions. However, the combination of studies on the behavior of Cs in anhydrous eclogite-melt systems, and the influence of water on partition coefficients, can provide some insight into the likely partition coefficient of Cs between eclogite and water-rich fluid.

A few studies evaluated the partition coefficient of Cs between garnet and/or clinopyroxene and silicate melt. Shimizu (1974) determined experimentally the partition coefficients of several trace elements, including Cs, between clinopyroxene and a silicate melt, $D_{Cs}^{cpx/melt}$, at pressures of 1.5–3 GPa and temperatures of 1100–1200 °C. He found values of 3.5 x 10^{-4} – 3.6 x 10^{-3}, with no significant correlation with either pressure or temperature in the range of conditions investigated. Klemme et al. (2002) studied experimentally the partition coefficients of trace elements between eclogitic mineralogy and anhydrous melt at 3 GPa and temperatures between 1100 and 1400 °C. They chose a Fe-free bulk composition thought to represent altered MORB in their experiments and mixed it with 22 trace elements including Cs. They determined $D_{Cs}^{cpx/melt} = 2.5 \times 10^{-3}$ and $D_{CS}^{grt/melt} = 1 \times 10^{-4}$ at 3 GPa and 1400 °C. They calculated bulk partition coefficients for eclogite, $D_{Cs}^{eclogite/melt}$, between 4×10^{-4} and 1.3×10^{-3} depending on the modal proportions of clinopyroxene and garnet in the rock. As indicated by Wood and Blundy (2002), the influence of water on the solidus of a system is significant, but its effect on partition coefficients of REE between garnet or pyroxene and melt is relatively small. We therefore assume the partition coefficient of Cs between eclogite and fluid to be on the order of 10^{-3}, supporting our assumption that >99.9% of the Cs added to the initial basaltic powder partitioned into the fluid during the experiments.

The amount of Cs in the fluid is known in each experiment based on the known amount of Cs-doped basalt. Cesium can, therefore, be used as an internal standard to calculate the concentration of all other elements in the fluid. The mass of each

element in the fluid is combined with the known mass of H_2O in each experiment to calculate the composition of the fluid. The average and standard deviation of three to seven analyses in each capsule are given in Table 4b. The standard deviation on the average amount of H_2O ranges between 1.9 and 8.5%, similar to the standard deviation on the average fluid composition calculated in the "evaporation" approach.

Uncertainties in the fluid composition in this approach were calculated by propagating errors on the amount of Cs (5%) and H_2O (3%). Two sets of 10000 random numbers were used to recalculate the amount of water and powder in each experiment according to the uncertainties estimated for each parameter. The uncertainties on the amount of H_2O and Cs in each experiment lead to uncertainty on the amount of H_2O in the fluid ranging from 0.7 to 2.5%, which are similar to (or smaller than) the standard deviation of the average of analyses in each experiment.

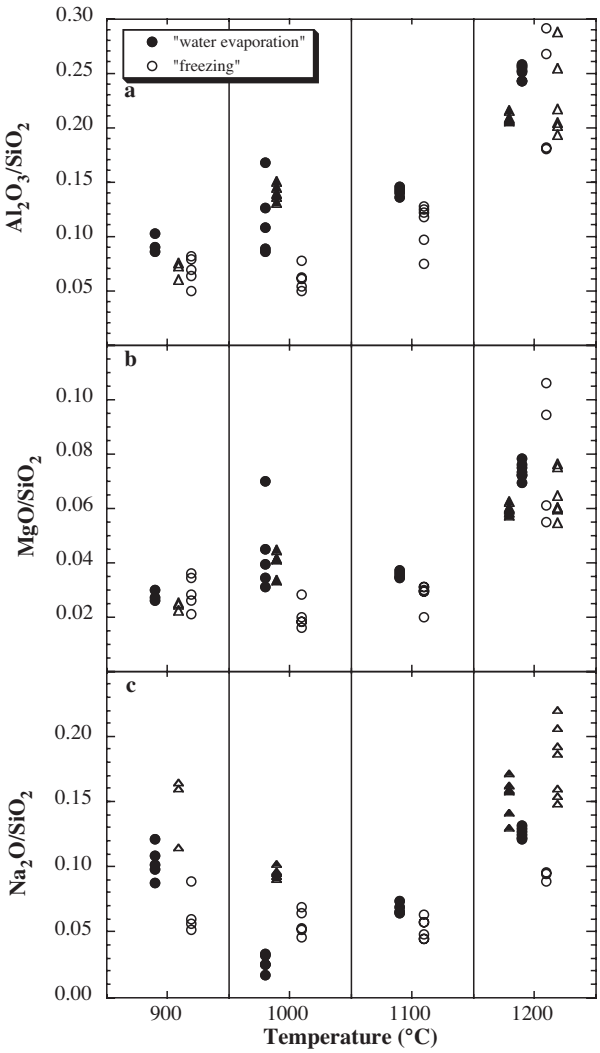

FIGURE 4. Comparison of oxide (wt%) ratios in fluids between capsules analyzed following the "evaporation" approach (filled symbols) and those analyzed by the "freezing" approach (open symbols) at each temperature. Each symbol represents a single LA-ICP-MS analysis in the diamond layer. (**a**) Al_2O_3/SiO_2. (**b**) MgO/SiO_2. (**c**) Na_2O/SiO_2.

COMPARISON BETWEEN "EVAPORATION" AND "FREEZING" APPROACHES

A total of twelve experiments were performed, six were analyzed following the "evaporation" approach and six following the "freezing" approach (Table 2). Figures 4 and 5 compare the fluid compositions calculated by the two approaches for experiments run at identical conditions. In each analysis both diamonds and precipitates/fluid are ablated, so element ratios are the only accurate information initially provided. Figures 4a–c compare calculated oxide ratios in the fluid phase between capsules analyzed by the "freezing" approach to those analyzed by the "evaporation" approach at each temperature. Figures 5a–c compare the calculated wt% oxide in the fluid phase between the

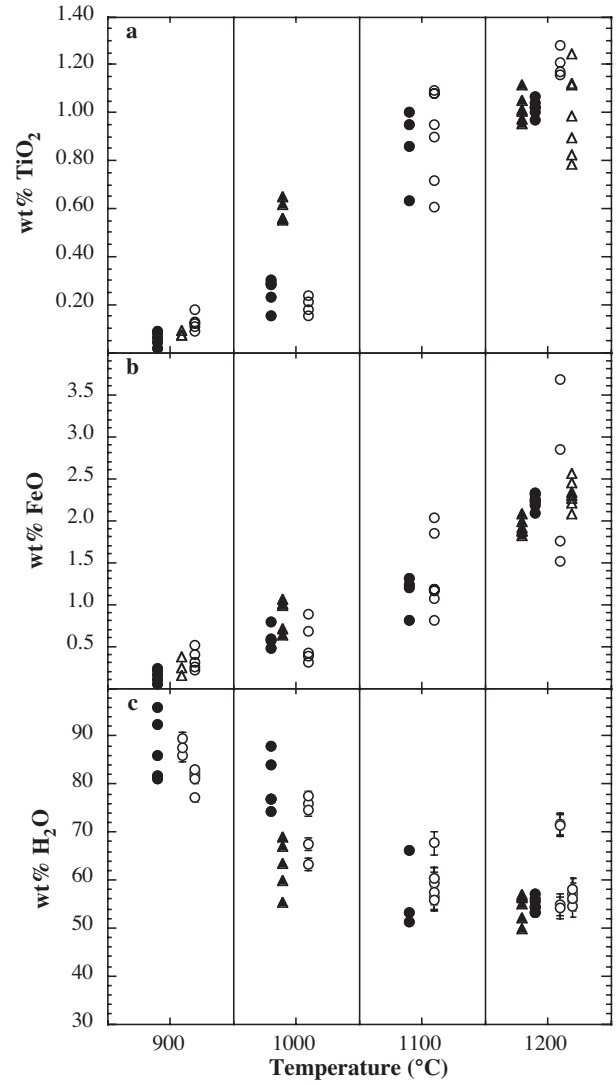

FIGURE 5. Comparison of wt% oxides in fluids between capsules analyzed following the "evaporation" approach and those analyzed by the "freezing" approach at several temperatures. Symbols as in Figure 4. (**a**) TiO_2. (**b**) FeO. (**c**) H_2O. Error bars (1σ) determined by propagating uncertainties are plotted for H_2O wt% calculated following the "freezing" approach.

two approaches. The oxide ratios and oxide concentrations in the fluids calculated by the two analytical approaches are in good agreement over the range of experimental temperatures.

The fluid compositions obtained in our study can be compared with those obtained by Stalder et al. (1998). They applied the diamond-trap technique to study trace-element partitioning between eclogitic minerals (garnet, clinopyroxene, coesite, rutile) in the CaO-MgO-Al_2O_3-SiO_2 system (Fe- and Na-free) and fluid at 3 and 5.7 GPa and temperatures between 900 and 1200 °C. The absolute oxide concentrations in that study were uncertain due to analytical difficulties, but oxide ratios in the fluid can be compared to those obtained in our study. The MgO/SiO_2 ratios in the aqueous fluids obtained by Stalder et al. (1998) vary between 0.11 and 0.99, much higher than those obtained in this study (0.02–0.11). All but one of the Stalder et al. (1998) experiments contained fluid coexisting with only a single phase, garnet or clinopyoxene, keeping the silica activity low. A single experiment contained coesite and clinopyroxene in the residual solid, i.e. was silica saturated, resulting in a significantly lower ratio of $MgO/SiO_2 = 0.11$, similar to values obtained for fluids in the present experiments. The fluid (MgO + FeO)/SiO_2 values obtained in our Ti-NCMFASH study vary between 0.03 and 0.26, well in the range of MgO/SiO_2 values obtained by Stalder et al. (1998) in the silica saturated runs in the CMASH system.

The Cs signal in the diamond trap including the frozen fluid (Fig. 3b) is an order of magnitude higher than in the signal in the diamond trap including precipitates only (Fig. 3a). The effects of variable dilution levels of the signal due to diamonds and the variable size of the ablation pits can be eliminated by comparing the ratio of Cs to one of the more refractory elements in the fluid. The Cs/Si ratio in the frozen fluid (Table 4b), for example, is an order of magnitude higher than this ratio in the precipitates (Table 4a). This observation suggests that the dominant fraction of Cs is not incorporated into the precipitates upon quenching but remains dissolved in the unmixed water. This observation is further supported when calculating the fluid composition in capsules treated following the "evaporation" approach using the Cs signal (Fig. 6a). Using the original amount of H_2O and Cs in each experiment, considerably lower concentrations of H_2O are calculated in the fluids compared to those obtained from mass balance. This comparison indicates a loss of between 71 and 98% of the amount of Cs during the evaporation of the water from the capsule. Cesium and K are both highly incompatible elements in mica-free eclogitic systems (Shimizu 1974; Klemme et al. 2002); therefore the loss of unquenched Cs with the water documented in the "evaporation" approach is to be expected and provides a first-order estimate of the loss of K in K-bearing experiments. Such systems, however, now can be studied using the "freezing" approach. Figure 6b provides a comparison of the fluid compositions in capsules treated following the "freezing" approach that were calculated using both calculation approaches—Cs signal and mass balance. The two independent calculation methods are in good agreement (Fig. 6b), thus validating the "freezing" approach.

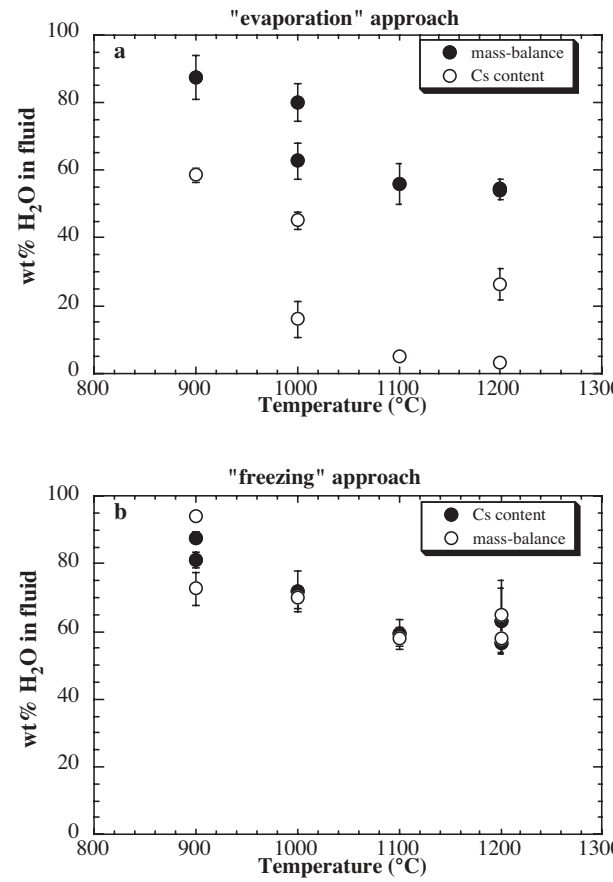

FIGURE 6. (a) The H_2O concentrations (wt%) of fluids in capsules treated following the "evaporation" approach obtained from mass balance compared to those calculated using the Cs signal. **(b)** The H_2O concentrations (wt%) of fluids in capsules treated following the "freezing" approach obtained by using the Cs signal compared to those based on mass balance calculations. Each symbol represents an average and one standard deviation of the distribution of analyses.

CONCLUDING REMARKS

The principal advantage of the "freezing" approach introduced in this work over the traditional "evaporation" approach is the possibility of studying fluid and hydrous melt compositions in equilibrium with mantle material regardless of chemistry. Potassium was previously shown to be highly soluble in water, even at room conditions, and thus to remain in the unmixed water evaporated prior to analyses (Stalder et al. 2002). The fluid composition in equilibrium with K-bearing rocks could not be studied experimentally until now using the traditional "evaporation" method. The knowledge of the composition of fluids that are either in equilibrium with eclogite (hydrated subducted oceanic crust) or with depleted and enriched upper mantle mineralogy is fundamental to understanding the generation of magmas from metasomatized upper mantle lithologies. Such material includes magmas ranging from arc-related basalts to "exotic" magmas such as kimberlites, lamproites, and carbonatites.

The "freezing" approach can be applied with an appropriate internal standard to convert the element ratios to absolute concentrations. For any given system, a highly incompatible element should be added to the starting material so its mass in the fluid at any experimental condition is known. An additional advantage of the "freezing" approach is the considerably lower

uncertainty in the results compared to those calculated following the "evaporation" approach. Although the compositions of the residual mineral phases are needed for the mass-balance calculations to determine the fluid composition following the "evaporation" approach (introducing large uncertainties), only the LA-ICP-MS analyses are required in the "freezing" approach. The "freezing" approach in conjunction with LA-ICP-MS now allows the study of HP-HT fluid and hydrous melt composition in equilibrium with any solid residue regardless of the chosen bulk composition.

ACKNOWLEDGMENTS

This work was supported by Swiss National Foundation (2000–61894.00/1). We thank Roland Stalder for advice and discussions throughout the study. Maik Pertermann is thanked for his help with the SEM work. The authors thank James Brenan and an anonymous reviewer for their constructive comments.

REFERENCES CITED

Baker, M.B. and Stolper, E.M. (1994) Determining the composition of high-pressure mantle melts using diamond aggregates. Geochimica et Cosmochimica Acta, 58, 2811–2827.

Bose, K. and Ganguly, J. (1995) Quartz-coesite transition revisited: Reversed experimental determination at 500–1200°C and retrieved thermochemical properties. American Mineralogist, 80, 231–238.

Brenan, J.M. and Watson, E.B. (1991) Partitioning of trace elements between olivine and aqueous fluids at high *P-T* conditions: implications for the effect of fluid composition on trace element transport. Earth and Planetary Science Letters, 107, 672–688.

Ghiorso, M.S. and Sack, R.O. (1995) Chemical mass transfer in magmatic processes IV. A revised and internally consistent thermodynamic model for the interpolation and extrapolation of liquid-solid equilibria in magmatic systems at elevated temperatures and pressures. Contributions to Mineralogy and Petrology, 119, 197–212.

Green, T.H., Blundy, J.D., Adam, J., and Yaxley, G.M. (2000) SIMS determination of trace element partition coefficients between garnet, clinopyroxene and hydrous basaltic liquids at 2–7.5 GPa and 1080–1200°C. Lithos, 53, 165–187.

Günther, D., Frischnecht, R., Heinrich, C.A., and Kahlert, H.J. (1997) Capabilities of an Argon Fluoride 193 nm excimer laser for laser ablation inductively coupled plasma mass spectrometry microanalysis of geological materials. Journal of Analytical Atomic Spectrometry, 12, 939–944.

Haifei, Z. (1996) Experimental study of the influence of hydrous minerals on the melting behaviour of rocks at high temperatures and pressures. Acta Geologica Sinica, 9, 157–167.

Halter, W.E., Pettke, T., Heinrich, C.A., and Rothen-Rutishauser, B. (2002) Major to trace element analysis of melt inclusions by laser-ablation ICP-MS: methods of quantification. Chemical Geology, 183, 63–86.

Harris, D.M. and Anderson, A.T. (1984) Volatiles H_2O, CO_2, and Cl in a subduction related basalt. Contributions to Mineralogy and Petrology, 87, 120–128.

Hawkesworth, C.J., Gallagher, K., Hergt, J.M., and McDermott, F. (1993) Mantle and slab contributions in arc magmas. Annual Review of Earth and Planetary Science, 21, 175–204.

Izraeli, E.S., Harris, J.W., and Navon, O. (2001) Brine inclusions in diamonds: a new upper mantle fluid. Earth and Planetary Science Letters, 187, 323–332.

Kessel, R., Beckett, J.R., and Stolper, E.M. (2001) Thermodynamic properties of the Pt-Fe system. American Mineralogist, 86, 1003–1014.

Klemme, S., Blundy, J.D., and Wood, B.J. (2002) Experimental constraints on major and trace element partitioning during partial melting of eclogite. Geochimica et Cosmochimica Acta, 66, 3109–3123.

Konzett, J., Sweeney, R.J., Thompson, A.B., and Ulmer, P. (1997) Potassium amphibole stability in the upper mantle: an experimental study in a peralkaline KNCMASH system to 8.5 GPa. Journal of Petrology, 38, 537–568.

Kress, V.C. and Carmichael, I.S.E. (1988) Stoichiometry of iron oxidation reaction in silicate melts. American Mineralogist, 73, 1267–1274.

Kushiro, I. and Hirose, K. (1992) Experimental determination of composition of melt formed by equilibrium partial melting of peridotite at high pressures using aggregates of diamond grains. Proceedings of the Japan Academy, 68, 63–68.

Longerich, H.P., Jackson, S.E., and Günther, D. (1996) Laser ablation inductively coupled plasma mass spectrometric transient signal data acquisition and analyte concentration calculation. Journal of Analytical Atomic Spectrometry, 11, 899–904.

Manning, C.E. (1994) The solubility of quartz in H_2O in the lower crust and upper mantle. Geochimica et Cosmochimica Acta, 58, 4831–4839.

McCulloch, M.T. and Gamble, J.A. (1991) Geochemical and geodynamical constraints on subduction zone magmatism. Earth and Planetary Science Letters, 102, 358–374.

Pettke T., Heinrich C.A., Ciocan A.C., and Günther D. (2000) Quadrupole mass spectrometry and optical emission spectroscopy: detection capabilities and representative sampling of short transient signals from laser-ablation. Journal of Analytical Atomic Spectrometry, 15, 1149–1155.

Rapp, R.P. and Watson, E.B. (1995) Dehydration melting of metabasalt at 8-32 kbar: implications for continental growth and crust-mantle recycling. Journal of Petrology, 36, 891–931.

Ryabchikov, I.D. and Boettcher, A.L. (1980) Experimental evidence at high pressure for potassic metasomatism in the mantle of the Earth. American Mineralogist, 65, 915–919.

Scambelluri, M. and Philippot, P. (2001) Deep fluids in subduction zones. Lithos, 55, 213–227.

Schmidt, M.W. and Poli, S. (1998) Experimentally based water budgets for dehydrating slabs and consequences for arc magma generation. Earth and Planetary Science Letters, 163, 361–379.

Schmidt, M.W. and Ulmer, P. (2004) A rocking multi-anvil: elimination of chemical segregation in fluid-saturated high pressure experiments. Geochimica et Cosmochimica Acta, 68, 1889–1899.

Shimizu, N. (1974) An experimental study of the partitioning of K, Rb, Cs, Sr, and Ba between clinopyroxene and liquid at high pressures. Geochimica et Cosmochimica Acta, 38, 1789-1798.

Stalder, R. and Ulmer, P. (2001b) Phase relations of a serpentine composition between 5 and 14 GPa: significance of clinohumite and phase E as water carriers into the transition zone. Contributions to Mineralogy and Petrology, 140, 670–679.

Stalder, R., Foley, S.F., Brey, G.P., and Horn, I. (1998) Mineral-aqueous fluid partitioning of trace elements at 900–1200°C and 3.0–5.7 GPa: New experimental data for garnet, clinopyroxene, and rutile, and implications for mantle metasomatism. Geochimica et Cosmochimica Acta, 62, 1781–1801.

Stalder, R., Ulmer, P., Thompson, A.B., and Günther, D. (2000) Experimental approach to constrain second critical end points in fluid/silicate system: Near-solidus fluids and melts in the system albite-H_2O. American Mineralogist, 85, 68–77.

Stalder, R., Ulmer, P., Thompson, A.B., and Günther, D. (2001) High pressure fluids in the system MgO-SiO_2-H_2O under upper mantle conditions. Contributions to Mineralogy and Petrology, 140, 607–618.

Stalder, R., Ulmer, P., and Günther, D. (2002) Fluids in the system forsterite-phlogopite-H_2O at 60 kbar. Schweizerische Mineralogische und Petrographische Mitteilungen, 82, 15–24.

Stern, C.R. and Wyllie, P.J. (1978) Phase compositions through crystallization intervals in basalt-andesite-H_2O at 30 kbar with implications for subduction zone magmas. American Mineralogist, 63, 641–663.

Stolper, E. and Newman, S. (1994) The role of water in the petrogenesis of Mariana trough magmas. Earth and Planetary Science Letters, 121, 293–325.

Susaki, J., Akaogi, M., Akimoto, S., and Shimomura, O. (1985) Garnet-perovskite transformation in $CaGeO_3$: in situ X-ray measurements using synchrotron radiation. Geophysical Research Letters, 12, 729–732.

Truckenbrodt, J., Ziegenbein, D., and Johannes, W. (1997) Redox conditions in piston-cylinder apparatus: The different behavior of boron nitride and unfired pyrophyllite assemblies. American Mineralogist, 82, 337–344.

Walker, D. (1991) Lubrication, gasketing, and precision in multianvil experiments. American Mineralogist, 76, 1092–1100.

Walker, D., Carpenter, M.A., and Hitch, C.M. (1990) Some simplifications to multianvil devices for high pressure experiments. American Mineralogist, 75, 1020–1028.

Wood, B.J. and Blundy, J.D. (2002) The effect of H_2O on crystal-melt partitioning of trace elements. Geochimica et Cosmochimica Acta, 66, 3647–3656.

Wyllie, P.J. and Ryabchikov, I.D. (2000) Volatile components, magmas, and critical fluids in upwelling mantle. Journal of Petrology, 41, 1195–1206.

Yagi, T. and Akimoto, S.-I. (1976) Direct determination of coesite-stishovite transition by in-situ x-ray measurements. Tectonophysics, 35, 259–270.

Yagi, T., Akaogi, M., Shimomura, O., Suzuki, T., and Akimoto, S.-I. (1987) In situ observation of the olivine-spinel phase transformation in Fe_2SiO_4 using synchrotron radiation. Journal of Geophysical Research, 92, 6207–6213.

Yaxley, G.M. and Green, D.H. (1998) Reactions between eclogite and peridotite: mantle refertilisation by subduction of oceanic crust. Schweizerische Mineralogische und Petrographische Mitteilungen, 78, 243–255.

Yoder, H.S. and Kushiro, I. (1969) Melting of a hydrous phase—phlogopite. American Journal of Science, 267, 558.

MANUSCRIPT RECEIVED SEPTEMBER 18, 2003
MANUSCRIPT ACCEPTED MARCH 12, 2004
MANUSCRIPT HANDLED BY MARC HIRSCHMANN